Journal of Advanced Ceramics
2018, **7**(4): 289–306
https://doi.org/10.1007/s40145-018-0287-z

ISSN 2226-4108
CN 10-1154/TQ

Review

Recent development of $A_2B_2O_7$ system transparent ceramics

Zhengjuan WANG[a,b,*], Guohong ZHOU[a,b,*], Danyu JIANG[a], Shiwei WANG[a,b,*]

[a]*State Key Laboratory of High Performance Ceramics and Superfine Microstructure, Shanghai Institute of Ceramics, Chinese Academy of Sciences, Shanghai 200050, China*
[b]*Key Laboratory of Transparent Opto-functional Inorganic Materials, Shanghai Institute of Ceramics, Chinese Academy of Sciences, Shanghai 200050, China*

Received: June 11, 2018; Accepted: June 19, 2018

Abstract: $A_2B_2O_7$ system compounds, which usually present three phase structures mainly based on the ionic radius ratios of r_A and r_B (r_A/r_B), have been studied for potential applications in many fields, such as thermal barrier coatings, luminescence powders, fast-ion conductors, photocatalysts, and matrices for immobilization of highly active radionuclides. Since 2005, $La_2Hf_2O_7$ was fabricated into transparent ceramics and much more attentions were paid on $A_2B_2O_7$ transparent ceramics for new applications. In this review, the development of $A_2B_2O_7$ system transparent ceramics was described. The structure characteristics, powder synthesis method, and sintering techniques of the final $A_2B_2O_7$ transparent ceramics were summarized. After that, the mostly reported $A_2Hf_2O_7$, $A_2Zr_2O_7$, and $A_2Ti_2O_7$ system transparent ceramics were systematically introduced. The potential application fields and future development trends were also discussed, focusing on scintillators, optical elements, and other luminescent materials.

Keywords: $A_2B_2O_7$ system transparent ceramics; powder synthesis; sintering; potential applications

1 Introduction

Since the 1950s, the first translucent Al_2O_3 was reported [1], and many transparent ceramics were developed, including oxide/non-oxide transparent ceramics, such as MgO [2], Y_2O_3 [3], CaO [4], BeO [5], ZrO_2 [6], $MgAl_2O_4$ [7], $LiAl_5O_8$ [8], Gd_2O_3 [9], Lu_2O_3 [10,11], $Y_3Al_5O_{12}$ [12,13], PLZT ($Pb_{1-x}La_x(Zr_yTi_z)O_3$) [14], $(Y,Gd)_2O_3$:Eu [15,16], Gd_2O_2S:Pr [17,18], $Gd_3Ga_5O_{12}$:Cr,Ce [19], and CaF_2 [20], MgF_2 [21], SrF_2 [22], BaF_2 [23], AlN [24], AlON [25,26], SiAlON [27], ZnS [28], ZnSe [29], CdTe [30], etc. They have been used or have potential applications in many fields, such as high pressure sodium lamp, ceramic metal halide lamp, filament of LED, high refractive index camera lens, bulletproof windows, or missile radome. Some of them possess opto-functional properties after doping with rare earth elements and can be used as laser media and scintillator in X-CT or PET.

$A_2B_2O_7$ system materials have been studied as early as in the 1960s [31], but they were used as thermal barrier coatings [32], luminescence powders [33,34], fast-ion conductors [35,36], photocatalysts [37], matrices for immobilization of highly active radionuclides [38–40], and so on, while the study on $A_2B_2O_7$ system transparent ceramics was kicked off in the 2000s. Their mainly potential applications are scintillator hosts as most of

* Corresponding authors.
E-mail: Z. Wang, wzhj926@mail.sic.ac.cn;
G. Zhou, sic_zhough@mail.sic.ac.cn;
S. Wang, swwang51@mail.sic.ac.cn

them have high density and effective atomic number, which would gain higher X-ray or γ-ray stopping power. Then, many transparent ceramics with the composition of $A_2B_2O_7$ were fabricated in recent years, such as $La_2Hf_2O_7$ [41,42], $La_{2-x}Gd_xHf_2O_7$ [43,44], $La_2Zr_2O_7$ [45], $Nd_2Zr_2O_7$ [46], $La_{2-x}Gd_xZr_2O_7$ [47,48], $La_{2-x}Lu_xZr_2O_7$ [49], and $Lu_2Ti_2O_7$ [50]. Also, rare earth ion doped $A_2B_2O_7$ system transparent ceramics [42,51–54] were fabricated to study their luminescent properties.

In this review, the structure characteristics, powder synthesis and ceramic sintering method, and potential applications of $A_2B_2O_7$ system transparent ceramics were systematically introduced. Finally, the development trends were described.

2 Structure characteristics

The crystal structure of $A_2B_2O_7$ compounds depends on ionic radius ratio of r_A and r_B (r_A/r_B), temperature, and pressure. The most commonly seen structures are cubic pyrochlore and defective fluorite phases, and sometimes monoclinic phase exists. In general, r_A/r_B is the most important factor. According to Subramanian *et al.* [55], pyrochlore structure steadily exists when r_A/r_B = 1.46–1.78, where A and B ions are distributed in order. Anion-deficient fluorite is the stable structure when r_A/r_B < 1.46, and the arrangement of A and B ions is disordered, while the monoclinic structure is stable when r_A/r_B > 1.78.

Figure 1 shows the crystal structure diagram of pyrochlore and defective fluorite [56]. Ideal pyrochlore structure is a super structure derivative of the simple fluorite structure (AO_2), where A and B cations are ordered along the <110> direction and one-eighth of the oxygen ions are absent. It can be written as $A_2B_2O_6O'$ and belongs to the space group $Fd\bar{3}m$ (Z = 8). The A, B, O, O′ ions occupy 16c, 16d, 48f, and 8b four crystalline sites, respectively. The unoccupied 8a site corresponds to the oxygen vacancy. As the oxygen vacancy resides in the tetrahedral interstitial site between adjacent B-site cations which reduces the coordination number of B cation from 8 to 6, while the coordination number of A cation is still 8 [40,57–59]. The defective fluorite structure exhibits the $Fm\bar{3}m$ (Z = 1) space group, and the arrangement of the cations and the distribution of the oxygen vacancies become disordered. In XRD patterns, the existence of diffraction peaks corresponding to (331) and (511) reflections is

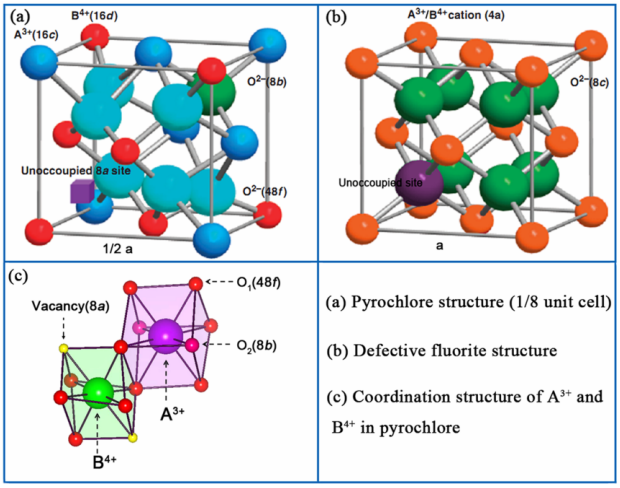

Fig. 1 Crystal structures of pyrochlore and defective fluorite: (a) one-eighth of unit cell of pyrochlore structure; (b) defective fluorite structure; (c) coordination structure of A^{3+} and B^{4+} in pyrochlore. Reproduced with permission from Ref. [56], © University of Chinese Academy of Sciences 2015.

always considered as a characteristic of the pyrochlore structure, which is a mark to be used to distinguish pyrochlore from defective fluorite structure. However, these characteristic peaks are intrinsically of low intensity [33].

3 Synthesis methods of $A_2B_2O_7$ powders

To date, the reported $A_2B_2O_7$ system transparent ceramics mainly include the compounds with A = La, Gd, Yb, Lu, Y, and B = Hf, Zr, Ti, Sn [60]. Most of the studies were in experimental stage, and focused on powder synthesis and ceramic sintering. There are many methods that have been used to synthesize $A_2B_2O_7$ powders, like the solid state method, hydrothermal process and solvothermal synthesis, molten salt synthesis, co-precipitation method, sol–gel process (including the stearic acid method and Pechini method), and combustion method. The progress of powder synthesis of $A_2B_2O_7$ system transparent ceramics is summarized in this part.

3.1 Solid state method

Solid state method is a conventional method for preparation of oxide powders; it is simple and applicable for many compounds including simple and complex compounds.

In 2006, a series of compositions with the general formula $RE_2Hf_2O_7$ (RE = Dy, Ho, Er, Tm, Lu, Y) were prepared by a standard solid state route and characterized

by powder XRD and Raman spectroscopy [61]. AR grade RE_2O_3 (RE = La, Nd, Sm, Dy, Ho, Er, Tm, Lu, Y) and HfO_2 were first heated at 900 ℃ overnight to remove moisture and other volatile impurities. Then stoichiometric amounts of the reactants were weighed and mixed to get the compositions corresponding to $RE_2Hf_2O_7$. And the mixtures were subjected to a three-step heating protocol (1200 ℃ 36 h–1300 ℃ 36 h–1400 ℃ 48 h) as followed with intermittent grindings. Subsequently, one more heat treatment at 1700 ℃ for 6 h was given to each sample to investigate the existence of pyrochlore structure. The Raman and XRD results showed that $RE_2Hf_2O_7$ (RE = La, Nd, Sm) crystallized in fully ordered pyrochlore phase, while $RE_2Hf_2O_7$ (RE = Ho, Er, Tm, Lu, Y) were unequivocally defect-fluorites. In the case of $Dy_2Hf_2O_7$, there was competition between defect-fluorite and pyrochlore lattices. This conventional solid state synthesis method involves many cycles of grinding of the component oxides and heating at high temperatures, and usually yields inhomogeneous complex oxides. Thus, some researchers developed a mechano-chemical synthesis method, which was a modified solid state reaction method, and usually long time ball milling was required to obtain single phase compounds. In 2005, $A_2(Ti_{(1-y)}Zr_y)_2O_7$ ($A = Gd^{3+}$, Y^{3+}) powders with pyrochlore structure were obtained by this mechano-chemical synthesis method [62]. Stoichiometric mixtures of the constituent oxides were milled in a planetary ball mill with a speed of 350 rpm. XRD results showed that chemical changes occurred in the powder mixtures after milling for 19 h, and single phase solid solutions were obtained. The powders were examined by SEM and found that they were basically consisted of submicron-sized agglomerates and aggregates of nanoparticles. As this method did not require post calcination process, it was relatively simpler than the traditional solid state reaction and the powders obtained were much finer. In 2006, $Gd_2(Sn_{1-y}Zr_y)_2O_7$ solid solutions with pyrochlore structure were also synthesized by this method [63]. XRD patterns showed the milled samples were similar to that of an anion deficient fluorite or to that of highly disordered pyrochlore but with weak superstructure reflections. All the samples became pyrochlore structure when calcined at 1450 ℃. That is to say, to obtain powders with high crystallinity, high temperature calcination is still required.

As solid state method usually needs long synthesis time and higher temperature, and the synthesized powders have wide particle size distribution and large particle size with low sintering activity, researchers have moved to wet chemical synthesis routes in order to prepare pure and homogeneous $A_2B_2O_7$ powders. In this case, powders at submicron or even nanometer scales can be obtained with significantly improved sintering activity.

3. 2 Hydrothermal method and solvothermal synthesis

Hydrothermal synthesis has been used to produce ceramic nanopowders with high crystallinity, high chemical homogeneity, and more stoichiometric. To date, $Ln_2Sn_2O_7$ (Ln = La, Y, Lu, Gd) nanocrystals [64] and $Y_2Zr_2O_7$:Tb^{3+} powders [65] were prepared by this method. Take $Y_2Sn_2O_7$:Yb^{3+} as an example to illustrate the detailed hydrothermal synthesis procedure. First, yttrium nitrate salt was dissolved in distilled water to form 0.1 mmol/L solution. Then certain amount of $Yb(NO_3)_3$ was added into the above solution under magnetic stirring condition. Keep the stirring for several minutes until the solution turned to uniformity, then 0.1 mmol/L sodium stannate was added into the solution and white precipitate was formed. The above solution was transferred into a Teflon-lined stainless steel autoclave and heated at 180 ℃ for 18 h, and naturally cooled to room temperature. The product was collected by centrifugation, washed with distilled water and alcohol for several times, and dried at 60 ℃ for 24 h in air. XRD patterns showed that all the obtained powders had cubic pyrochlore structure.

Also, solvothermal synthesis of $Y_2Ti_2O_7$:Eu^{3+} sphere powders was reported by Pavitra *et al.* [66] in 2013. Organic solvent (2-propanol) was chosen as the solvent instead of water. Yttrium nitrate, titanium isopropoxide, and europium nitrate were the raw materials. The specific synthesis process was similar to the hydrothermal method.

The above experiments showed that hydrothermal method and solvothermal synthesis are energy conservative methods to obtain $A_2B_2O_7$ powders with pure phase composition at low temperature. Besides, the phase composition, particle size, and morphology, etc., can be controlled by adjusting the precursor concentration, reaction temperature and pressure, holding time, and additives.

3. 3 Molten salt synthesis method

The molten salt synthesis (MSS) is intrinsic simple, versatile, and cost-effective. It can be used to prepare

chemically purified, single phase powders at lower temperature and often in overall shorter reaction time with little residual impurities as compared with conventional solid state reactions. Thus, it was attractive by many researchers to prepare a wide range of complex oxide nanocrystals [67]. Usually, one salt (e.g., NaCl) or a eutectic mixture of salts (e.g., NaCl/KCl; $NaNO_3$/KNO_3) is chosen as the molten salt medium. In 2009, Mao *et al.* [68] prepared nanocrystals with $A_2B_2O_7$ (A = La, Er, or their mixture; B = Zr, Hf, or their mixture) composition by this method. First, a single-source complex precursor $A(OH)_3{\cdot}BO(OH)_2{\cdot}nH_2O$ was prepared via co-precipitation of $A(NO_3)_3$ and $BO(NO_3)_2$/$BOCl_2$ in a dilute ammonia solution at room temperature. The precursor complex was then purified by filtration and washing with water. After being air-dried for 24 h, the complex precursor was mixed with nitrate mixture ($NaNO_3$:KNO_3 = 1:1). The mixture was transferred into a covered nickel crucible and heated to 650 ℃ at 10 ℃/min and then isothermally annealed at 650 ℃ for 6 h. After being cooled to room temperature, the resulting product was centrifuged and purified with deionized water several times. After drying, $A_2B_2O_7$ nanocrystals were obtained.

In this method, the precursor molecules disperse, dissociate, rearrange, and then diffuse rapidly throughout the salt medium at high temperature. The desired oxide phase is formed through an initial nucleation step followed by a growth process. Thus, relatively homogeneous powders can be obtained.

3. 4 Co-precipitation method

Co-precipitation method is a simple, inexpensive, and quick way to synthesize various oxide powders. Usually, chloride, nitrate, or oxychloride, etc., were used as the initial reactants, and ammonia, ammonium bicarbonate, or oxalate were used as the precipitant. Typically, precipitates are prepared and then the target oxide products are obtained by a subsequent calcination process. In previous works, $Ln_2Ti_2O_7$ (Ln = Lu, Gd, Yb, Tm) [69,70], $(La_xGd_{1-x})_2Zr_2O_7$ [71], $(Nd_xGd_{1-x})_2Zr_2O_7$ [72], $Y_2Hf_2O_7$ [73], and $Gd_2Hf_2O_7$:Ce [74] powders were prepared by co-precipitation method. The morphology of the ceramic powders can be modified by adding surfactant [73]. Zhou *et al.* [73] prepared $Y_2Hf_2O_7$ powders by oxalate co-precipitation method, and different shapes such as platelet, rod, and spherical shape were obtained by controlling the concentration of the surfactant PEG6000 (Fig. 2).

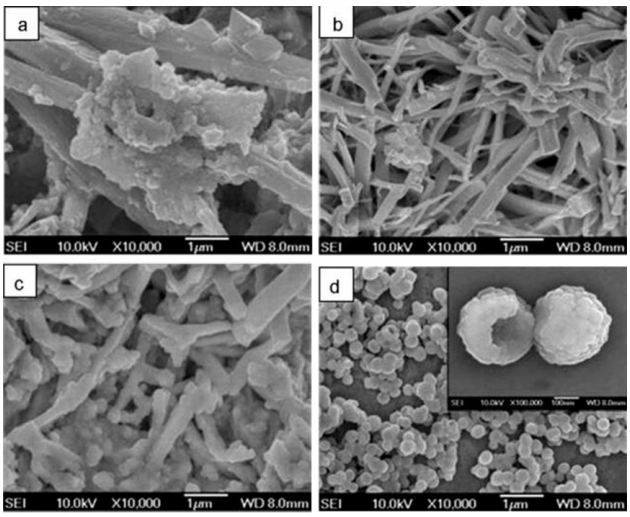

Fig. 2 $Y_2Hf_2O_7$ powders prepared with different concentrations of surfactant: (a) 0%, (b) 0.6%, (c) 1.2%, (d) 1.5%, and calcined at 800 ℃ for 2 h. Reproduced with permission from Ref. [73], © Elsevier B.V. 2009.

Though various morphologies can be obtained by co-precipitation method, agglomeration is inevitably observed in powders synthesized by this method, which is harmful for the sintering of transparent ceramics.

3. 5 Sol–gel method

The sol–gel method offers considerable advantages of good mixing of the starting materials and excellent chemical homogeneity and phase purity of the synthesized powders. The molecular level mixing and the tendency of partially hydrolyzed species to form extended networks facilitate the structure evolution thereby lowering the crystallization temperature. Thus, it makes the preparation of particular phases possible at ambient and gentle conditions. Usually, organic solvent and stabilizer, such as acetylacetone, 2-methoxyethanol, and methanol, are used. A subsequent calcination process is also necessary to obtain the target powders. $La_2Zr_2O_7$ and $La_{1.96}Eu_{0.04}Zr_2O_7$ [75], Er^{3+}-doped $La_2Ti_2O_7$ [76], and Eu^{3+}/$Y_2Ti_2O_7$ [77] powders were also examples synthesized by sol–gel method.

Stearic acid method (SAM) was a modified sol–gel method, in which stearic acid was used as solvent and dispersant. In 2008, cubic fluorite type $Y_2Zr_2O_7$ nanocrystal was synthesized by SAM using zirconium nitrate and yttrium nitrate as raw materials [78]. Pechini method was also a kind of sol–gel method. In 2010, undoped and Pr-doped $La_2Hf_2O_7$ nanopowders were synthesized by Pechini reaction method [34], and

pure cubic pyrochlore structure of $La_2Hf_2O_7$ was formed at 1000 ℃.

Comparatively, sol–gel method is too complex as it involves too many processes and is time-consuming [75]. Then, relatively simple experimental processes were developed; for instance, the combustion method.

3. 6 Combustion method

Combustion method is a simple and rapid method and is widely used to synthesize $A_2B_2O_7$ powders. The major advantages of the combustion process are: improvement in processing time, energy saving, and the high sintering activity of the combustion products. In this method, nitrate is the common raw material, and carbohydrazide [79], urea [79–81], glycine [41,80,82, 83], and ethylene diamine tetraacetic acid (EDTA) [41] or two of them are used as fuels. So far, $Ln_2Zr_2O_7$ (Ln = La, Ce, Pr, Nd, Sm, Gd, and Dy) [79], $La_2Zr_2O_7$ [81,82], $Y_2Zr_2O_7$ [83], $Nd_2Zr_2O_7$ [46], $La_{2-x}Gd_xZr_2O_7$ [47,48,54], $LaLuZr_2O_7$ [84], $LaYZr_2O_7$ [85], $La_2Hf_2O_7$ [41,51,52], $Y_2Hf_2O_7$ [86,87], $Lu_2Hf_2O_7$ [80], and $La_{2-x}Gd_xHf_2O_7$ [44] powders were synthesized by combustion method. The surface area, density, and morphology of the prepared powders are different when using different fuels [41,79,80]. It was attributed to the nature of the fuels that controls the energetics/ exothermicity of the combustion reaction [79]. In Liao *et al.*'s work [80], the effects of the fuel types and molar ratios of glycine-to-nitrate on the crystallinity and properties of $Y_2Hf_2O_7$ were investigated. It showed that the crystallite size increased with the value of f/o (fuel/oxidizer ratio) becoming close to stoichiometric ratio, resulting in the largest crystallite size at the stoichiometric ratio. The type of fuels can also affect the crystallinity and size of $Y_2Hf_2O_7$ powders. The crystallite size of the powders increases in the order of glycine, urea, and the mixed fuels. The sample produced by the mixed of fuels method has more uniform size distribution, less agglomeration for the change of the reducing power of the fuel and the chelating effect of EDTA, which was added as a complexant.

Powders synthesized by combustion method have the similar morphology with porous network structure and are severely agglomerated (shown in Fig. 3(a)) [47]. The porous network structures may be originated from the release of gases, such as CO_2, N_2, and H_2O during the combustion process. The subsequent ball milling process can remove the agglomeration and destroy the porous network structure (Fig. 3(b)). This is helpful for the densification process when the powders are sintered to transparent ceramics.

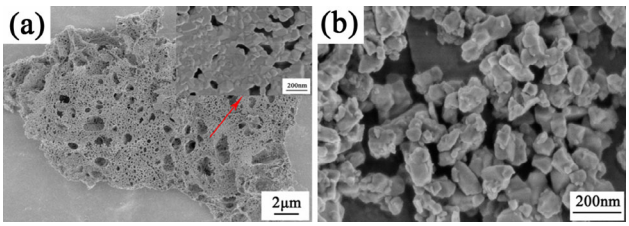

Fig. 3 Typical SEM images of powders synthesized by combustion method: (a) the as-burnt $LaGdZr_2O_7$ powders calcined at 800 ℃; (b) $LaGdZr_2O_7$ powders ball-milled for 20 h. Reproduced with permission from Ref. [47], © Elsevier Ltd. 2012.

In a word, $A_2B_2O_7$ powders were obtained by many synthesis methods mentioned above. Some of the methods are complex because of the addition of many organics. Combustion method is simple and rapid; it has been widely used to synthesize $A_2B_2O_7$ powders.

4 Sintering methods of $A_2B_2O_7$ transparent ceramics

The reported sintering methods for $A_2B_2O_7$ transparent ceramics included vacuum sintering, spark plasma sintering (SPS), hot isostatic pressing (HIP) sintering, and low-temperature high-pressure (LTHP) sintering.

4. 1 Vacuum sintering

Vacuum sintering [88] refers to a sintering process carried out in a vacuum equipment to achieve better results than those run at atmospheric pressure. Vacuum sintering is typically used to fabricate oxide transparent ceramics, like garnet [12], Y_2O_3 [3], Lu_2O_3 [10], and so on. The sintering temperature carried out is relatively high and usually 200 ℃ below the melting point of the ceramic body, while the vacuum sintering furnace is relatively cheap and the operation is simple. Also, no pressure is needed.

Most of the reported $A_2B_2O_7$ transparent ceramics were fabricated by vacuum sintering without any atmosphere. For example, $Y_2Hf_2O_7$ transparent ceramic [86] was fabricated by vacuum sintering. First, the cold isostatic pressed (CIPed) green body was pre-sintered at 1200 ℃ for 2 h to remove the residual organics originated from the forming process (compacting process). Then, the samples were vacuum sintered at 1800–1950 ℃ for 6 h with a vacuum degree of 10^{-3} Pa.

This method was also carried out to prepare transparent ceramics such as $Y_2Zr_2O_7$ [83], $La_{2-x}Gd_xZr_2O_7$ [47,48, 56], Eu^{3+}:$La_{2-x}Gd_xZr_2O_7$ [53], $La_{2-x}Lu_xZr_2O_7$ [49,84], $LaYZr_2O_7$ [85], $Y_2Hf_2O_7$ [87], $La_{2-x}Y_xHf_2O_7$ [90], $La_{2-x}Gd_xHf_2O_7$ [43,44], and Eu^{3+}:$La_{0.8}Gd_{1.2}Hf_2O_7$ [54].

Some of the $A_2B_2O_7$ transparent ceramics were fabricated by vacuum sintering in hydrogen or helium. $La_2Hf_2O_7$ [41], $Gd_2Hf_2O_7$ [89], $La_2Hf_2O_7$:Tb [51], $La_2Hf_2O_7$:Ti [52], and $Nd_2Zr_2O_7$ [46] transparent ceramics were all fabricated by sintering the compacted green body in H_2 atmosphere.

Usually, the post-annealing process is necessary for vacuum sintering of most transparent ceramics. After sintering in vacuum, oxygen vacancies would generate as the vacuum atmosphere is a kind of anoxic environment. As the oxygen vacancies can produce strong light absorption through the formation of color centers, which would lead to the coloration of the ceramics. The post-annealing process could supply oxygen from air and eliminate the coloration of the ceramics, so as to obtain higher transparency [53,54,56].

For this sintering method, the usual average grain sizes of single phase transparent ceramics were about several micrometers to tens of micrometers, and were relatively larger than other methods in which pressure is used, while the grain size would decrease when two phases coexisted in the transparent ceramics, like in $La_{2-x}Lu_xZr_2O_7$ system ceramics [49]. When x ranged from 0.6 to 1.2, pyrochlore and defective fluorite phases coexisted and the average grain sizes were only 2–5 μm.

4. 2 Spark plasma sintering

Spark plasma sintering (SPS) [88] is a method for obtaining fully dense and fine-grained transparent ceramics at low temperatures within short time durations. It is also known as field-assisted sintering or pulsed electric current sintering. SPS has been used to fabricate transparent ceramics because of its characteristic fast densification without significant grain growth. By controlling the sintering parameters, such as temperature, heating rate, pressure, dwell time, and atmosphere, highly transparent ceramics can be produced [91].

In 2011, An *et al.* [45,50] fabricated $La_2Zr_2O_7$ and $Lu_2Ti_2O_7$ transparent ceramics by reactive spark plasma sintering. The sintering temperature was as low as 1400 and 1500 ℃ respectively, with a pressure of 100 MPa and short holding time (45 min). However, the transmittance of the ceramics in the visible range was relatively low. As a graphite die was used in SPS, carbon contaminant was introduced and lowered the optical quality.

4. 3 Hot isostatic pressing sintering

For some transparent ceramics, simple vacuum sintering or pressureless sintering cannot produce high density, thus high external force is needed, like high pressure. Hot isostatic pressing (HIP) sintering becomes a good choice. HIP [88] is a manufacturing process used to achieve the maximum possible densification, which is a key to reach high light transmittance for transparent ceramics. To reduce the fabrication cost, HIP is usually used as the last step followed by vacuum sintering or pressureless sintering. It has been widely used to synthesize transparent armor ceramics, such as sub-micron grained alumina (Al_2O_3) [92] and spinel ($MgAl_2O_4$) [93]. Nowadays, HIP process was also used to prepare cubic sesquioxide ceramics, including Y_2O_3 [94], Sc_2O_3 [95], and Lu_2O_3 [11]. In these cases, vacuum sintering was first used to remove closed porosity, and then a subsequent HIP step was employed. HIP process can be also combined with hot pressing (HP). HP followed by HIP was proved to be more feasible to fabricate transparent $MgAl_2O_4$ ceramics.

As a high-cost sintering method, HIP sintering is not widely used in fabricating $A_2B_2O_7$ transparent ceramics. In Schott Company's US patent [96], solid state reactive sintering of $Y_2Ti_2O_7$ was carried out by vacuum sintering in hydrogen or helium at 1500 ℃ for 3 h and then HIP at 1700 ℃ for 1 h–Ar–200 MPa. Afterwards, the ceramics were reoxidized in a further thermal step (for example 900 ℃, 5 h, in air) and optically transparent and homogeneous bodies were obtained. $Yb_2Ti_2O_7$ transparent ceramic was also fabricated by similar process. In another US patent [74], $Gd_2Hf_2O_7$:Ce and other $A_2X_2O_7$ transparent ceramic scintillator bodies were sintered by two-step method. For $Gd_2Hf_2O_7$:Ce, the CIPed pellets were first sintered in air at 1500–1600 ℃ for 3 h, and then HIPed at 1400–1600 ℃ for 1 h in argon at approximately 30 ksi. To achieve high optical quality, the sintering technology still needs to be adjusted and optimized.

4. 4 Low-temperature high-pressure process

Low-temperature high-pressure (LTHP) process is similar to the HP process, but with higher pressure (in GPa grade). This method can be successfully applied for densification of nanocrystalline powders into transparent ceramics and is competitive to restrain the small grain

size in the product. For example, nanocrystalline $MgAl_2O_4$ and YAG transparent ceramics [97,98] were fabricated by this method. For $MgAl_2O_4$ nanocrystalline transparent ceramic, the optimal sintering condition has been determined to be around 620 ℃/3.7 GPa, and the average grain size was only about 61 nm. For Pr:YAG nanoceramic, the LTHP sintering condition was 450 ℃/8 GPa for 1 min with a transmittance of 51% at 1250 nm. The average grain size was only about 24 nm.

In 2014, Trojan-Piegza *et al.* [42] fabricated $La_2Hf_2O_7$:Pr transparent ceramic by LTHP sintering technique using nanopowders made by Pechini method. The CIPed pellets were sintered in a graphite die at a pressure ranging in the 2–8 GPa at different temperatures between 300 and 1500 ℃. And the time of sintering varied from 1 to 20 min. Results showed that the samples sintered at 1400 ℃ for 2 min and additionally at 900 ℃ for another 10 min in one continuous run were found to be of highest translucency. The average grain size of the samples was about 150 nm.

Though this method can obtain transparent nanoceramics, the transparency was not as good as transparent ceramics obtained by other sintering methods. If higher mechanical properties of the ceramics were required, this LTHP method is an option because of its significantly effect of restraining grain size.

5 $A_2B_2O_7$ system transparent ceramics with different compositions

For $A_2B_2O_7$ system transparent ceramics, the common forming method was dry pressing and cold isostatic pressing. Only a few researchers used the wet molding technique, like slip casting [85]. After sintered by different methods mentioned in the last part, $A_2B_2O_7$ system transparent ceramics were obtained. Fabrication method and properties of the reported $A_2B_2O_7$ system transparent ceramics are summarized in Table 1. In this

Table 1 Fabrication method and properties of the reported $A_2B_2O_7$ system transparent ceramics

Compound	Powder synthesis method	Sintering method	r_A/r_B	Crystal structure*	Density (g/cm^3)	Transmittance (%)	Refractive index
$La_2Hf_2O_7$ [41,89]	Combustion method	Pressureless sintering in H_2	1.63	P	7.93	> 70% (633 nm, 0.6 mm)	—
$Gd_2Hf_2O_7$ [89]	Combustion method	Pressureless sintering in H_2	1.483	P	9.38	> 70% (633 nm, 0.6 mm)	—
$Y_2Hf_2O_7$ [86]	Combustion method	Vacuum sintering	1.435	F	7.54	> 50% (633 nm, 1 mm)	—
$Y_2Hf_2O_7$ [87]	Solid state reactive method	Vacuum sintering	1.435	F	7.54	> 60% (633 nm, 1 mm)	2.018 (600 nm)
$La_{2-x}Y_xHf_2O_7$ [90]	Solid state method	Vacuum sintering	1.435–1.63	x < 0.4: F; $x \geqslant$ 0.4: P	7.54–7.93	x = 1.2: 75.3% (633 nm, 1 mm)	x = 1.2:2.04 (633 nm)
$LaGdHf_2O_7$ [43]	Solid state method	Vacuum sintering	1.56	P	8.37	74% (1100 nm, 1 mm)	—
$La_2Hf_2O_7$:Pr [42]	Pechini method	LTHP	—	P	7.74	~38% (900 nm, 1 mm)	—
$La_{2-x}Gd_xHf_2O_7$ [44]	Combustion method	Vacuum sintering	1.483–1.63	P	7.91–8.88	x = 1.2: 76.1% (800 nm, 1 mm)	~2.05 (633 nm)
$Gd_2Zr_2O_7$ [99]		Vacuum sintering + HIP	1.46	P	6.93	—	—
$La_2Zr_2O_7$ [45]		SPS	1.61	P	6.057	68% (4–6 μm, 1 mm)	—
$Y_2Zr_2O_7$ [83]	Combustion method	Vacuum sintering	1.42	F		68% (633 nm, 1 mm)	—
$Nd_2Zr_2O_7$ [46]	Combustion method	Pressureless sintering in H_2	1.54	P		> 60% (633 nm,1 mm)	—
$La_{2-x}Gd_xZr_2O_7$ [47,48]	Combustion method	Vacuum sintering	1.46–1.61	P	6.01–6.72	x = 0.4: 73.6% (1100 nm, 1 mm)	~2.08 (633 nm)
$La_{2-x}Lu_xZr_2O_7$ [49]	Solid state method	Vacuum sintering	1.36–1.61	x < 0.4: F; 0.4≤x≤1.2: P+F; $x \geqslant$ 1.4: F	5.94–7.84	x = 1.2: 72.4% (1100 nm, 1 mm)	—
$LaLuZr_2O_7$ [84]	Combustion method	Vacuum sintering	1.48	P + F	6.82	73.4% (1100 nm, 1 mm)	—
$LaYZr_2O_7$ [85]	Combustion method	Vacuum sintering	1.51	P	5.81	74.3% (633 nm, 1 mm)	2.07 (633 nm)
$Y_2Ti_2O_7$ [96]	Solid state method	Vacuum sintering + HIP	1.68	P	5.03	—	—
$Y_{2+x}Ti_2O_{7+3x/2}$ [102]	Solid state method	Vacuum sintering	1.68	P	99.89%	x = 0.04: 49.9% (1100 nm, 0.5 mm)	2.20 (560 nm)
$Lu_2Ti_2O_7$ [50]	Solid state method	SPS	1.61	P	99.7%	40% (550 nm, 1 mm)	2.57 (633 nm)

*P = pyrochlore; F = defective fluorite.

part, $A_2Hf_2O_7$, A_2ZrO_7, and $A_2Ti_2O_7$ three system transparent ceramics were mainly introduced.

5. 1 $A_2Hf_2O_7$ system transparent ceramics

The $A_2Hf_2O_7$ system transparent ceramics were first developed for the potential application as new scintillators. In 2003, a bright and fast luminescence, characterized by Ce^{3+} interconfiguration 5d→4f transition, was observed in Ce-doped $La_2Hf_2O_7$ compound (powders) obtained by solid state reaction [100]. Then, Ce:$La_2Hf_2O_7$ began to be paid much attention as a new heavy and fast scintillator. As the growth of large size $La_2Hf_2O_7$ single crystal was very difficult due to its high melting point, Ji *et al.* [41,89] successfully fabricated $La_2Hf_2O_7$ and $Gd_2Hf_2O_7$ transparent ceramics for the first time in 2005 (Fig. 4 and Fig. 5). The powders were synthesized by combustion method and the transparent ceramics were obtained by sintering at 1850 ℃ in H_2 atmosphere. However, fast decay derived from 5d→4f transition of Ce^{3+} was not observed, and many studies were carried out and got the same results, which was not consistent with Borisevich *et al.*'s research in 2003 [100]. Chaudhry *et al.* [57] proposed an idea in 2011 that Ce-doped $RE_2M_2O_7$ (RE = Y, La; M = Ti, Zr, Hf) were a class of non-scintillators. Basing on the first-principle, they performed electronic structure calculation of these compounds, and found that the Ce 5d state lies above the CBM (conduction band minimum) (Fig. 6), which would prevent any luminescence from the Ce site. These studies made the enthusiasm on research of this kind of transparent ceramics gradually decreased, especially on the fast decay scintillation applications with Ce^{3+} doping. The luminescence of Tb^{3+} in the A-site and Ti^{4+} in the Hf^{4+} site for $La_2Hf_2O_7$ ceramic was reported in 1984 [101], and the emission of $La_2Hf_{1.98}Ti_{0.02}O_7$ had an intensity of about 1.6 times that of PAR $CaWO_4$, which would be of interest as an X-ray intensifying screen phosphor. Thus, Ji *et al.* fabricated $La_2Hf_2O_7$:Tb [51] and $La_2Hf_2O_7$:Ti [52] transparent ceramics. The luminescence properties of these transparent ceramics were also studied. For $La_2Hf_2O_7$:Ti transparent ceramic, the broad emission band centered at 475 nm originated from the oxide-Ti^{4+} charge-transfer transitions, which rendered fast decay time on the order of 10 μs. It was comparable to that of Gd_2O_2S:Pr ceramic scintillator (3 μs) and much faster than that of $(Y,Gd)_2O_3$:Eu ceramic scintillator (1000 μs). The highest relative light output reached about 1.5 times that of $Bi_4Ge_3O_{12}$ (BGO) single crystal when excited by 120 kV X-rays. Thus, $La_2Hf_2O_7$:Ti transparent ceramic is very promising as scintillator materials for X-ray CT detector applications, while some other properties such as afterglow and radiation damage are also crucial for the X-ray CT imaging, but they were not studied further.

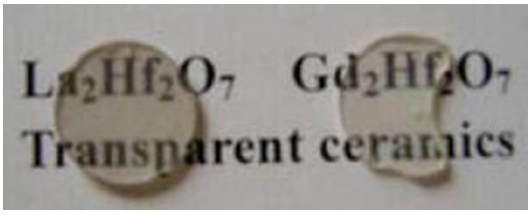

Fig. 4 Photograph of $Ln_2Hf_2O_7$ (Ln = La, Gd) ceramics sintered at 1850 ℃ for 6 h. Reproduced with permission from Ref. [89], © Chinese Academy of Sciences 2006.

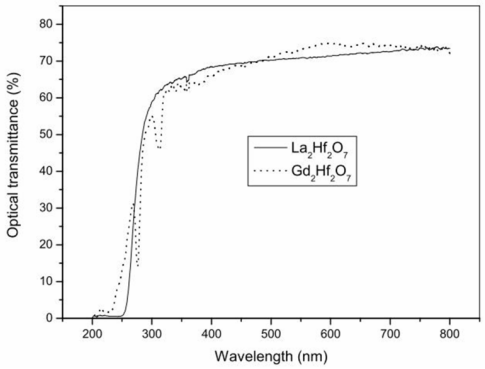

Fig. 5 Transmittance of $Ln_2Hf_2O_7$ (Ln = La, Gd) transparent ceramics sintered at 1850 ℃ for 6 h. Reproduced with permission from Ref. [89], © Chinese Academy of Sciences 2006.

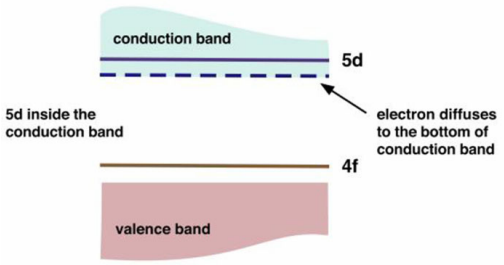

Fig. 6 Simple schematic model to illustrate the scenario for no Ce^{3+} luminescence: lowest Ce 5d inside the host conduction band. Reproduced with permission from Ref. [57], © American Institute of Physics 2011.

In 2011, Zou *et al.* [86] prepared $Y_2Hf_2O_7$ transparent ceramic by vacuum sintering. The $Y_2Hf_2O_7$ powders were synthesized by combustion method with EDTA as the fuel. The ceramic showed a transmittance of 50% (1 mm thick) in the visible spectral region. Further, Zhou *et al.* [87] optimized this process and the

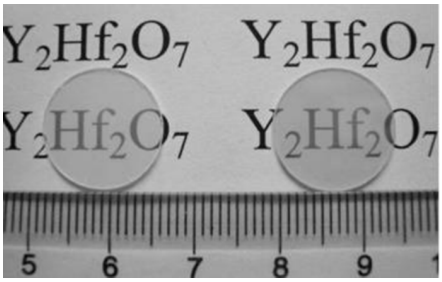

Fig. 7 Photograph of the mirror-polished $Y_2Hf_2O_7$ transparent ceramics (1 mm thick) sintered at 1900 ℃ for 6 h (left) and 12 h (right), respectively. Reproduced with permission from Ref. [87], © Elsevier B.V. 2012.

transmittance of the $Y_2Hf_2O_7$ ceramic (Fig. 7) was improved to 60% (1 mm thick) in the visible spectra region (Fig. 8). With the refractive index 2.018, the calculated theoretical transmittance was about 78.5%. That is, the prepared $Y_2Hf_2O_7$ transparent ceramic reached 76% of the theoretical transmittance.

$A_2Hf_2O_7$ transparent ceramics with two elements in A site were also studied. In 2011, $La_{2-x}Y_xHf_2O_7$ system transparent ceramics (Fig. 9) were fabricated [90] by solid state reaction sintering in vacuum at 1900 ℃, and phase transition (Fig. 10) occurred with the increase

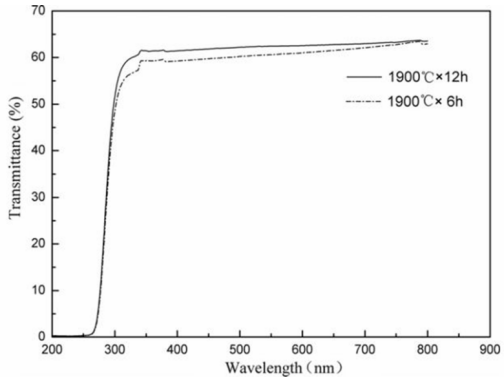

Fig. 8 Transmittance of the mirror-polished $Y_2Hf_2O_7$ transparent ceramics (1 mm thick). Reproduced with permission from Ref. [87], © Elsevier B.V. 2012.

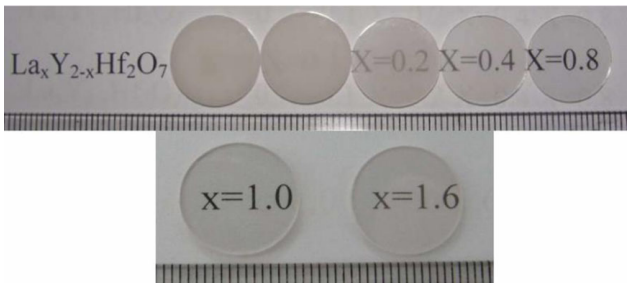

Fig. 9 Photograph of $La_{2-x}Y_xHf_2O_7$ ceramics (x = 0–1.6) (polished, 1 mm thick). Reproduced with permission from Ref. [90], © Chinese Academy of Sciences 2011.

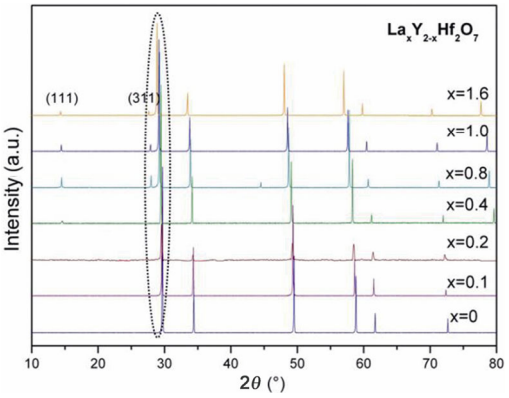

Fig. 10 XRD patterns of $La_{2-x}Y_xHf_2O_7$ ceramics (x = 0–1.6) sintered at 1900 ℃ for 6 h. Reproduced with permission from Ref. [90], © Chinese Academy of Sciences 2011.

of x. When x < 0.4, defective fluorite structure was presented, while pyrochlore structure showed up when $x \geqslant 0.4$. It was consistent with Subramanian *et al.*'s theory [55]. Meanwhile, Yi *et al.* [43] reported $LaGdHf_2O_7$ transparent ceramic, which was prepared by solid state method and vacuum sintering at 1900 ℃. The transmittance reached to 74% at 1100 nm.

Combined with the high density and effective atomic number, $La_{2-x}Y_xHf_2O_7$ and $LaGdHf_2O_7$ transparent ceramics were considered as promising candidates for scintillator host. However, the sintering temperature was so high that the energy consumption and equipment loss were large. Therefore, it is imperative to develop new methods to reduce the sintering temperature. In 2014, Trojan-Piegza *et al.* [42] fabricated $La_2Hf_2O_7$:Pr transparent ceramic by a new low-temperature high-pressure (LTHP) sintering method. The sintering temperature was as low as 1400 ℃, the holding time was 2 min, and the transmittance was very low (Fig. 11). Moreover, after annealing in air at 900 ℃ for 5 h, which was required to remove the dark color, the opacity enhanced unfortunately. The expected 5d–4f transition of Pr^{3+} was not detected and only 4f–4f transition was presented, indicating that fast decay also would not happen in $La_2Hf_2O_7$:Pr scintillator. In 2016, Wang *et al.* [44] reported the $La_{2-x}Gd_xHf_2O_7$ system transparent ceramics (Fig. 12). They were fabricated through vacuum sintering from nanopowders synthesized by combustion method. All the ceramics were transparent after being sintered at 1830 ℃ for 6 h, and the sintering temperature was lower than that of Yi *et al.*'s [43] work, indicating that powders synthesized by combustion method have higher sintering activity and can effectively lower the sintering temperature. The highest in-line transmittance was 76.1% at 800 nm

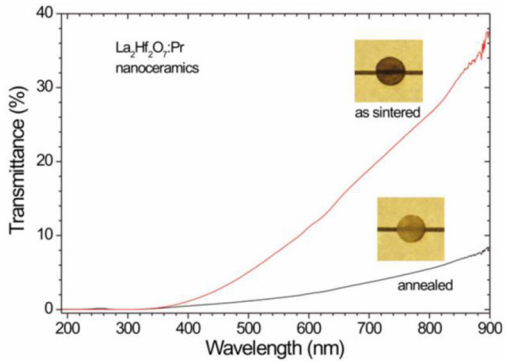

Fig. 11 Transmittance of $La_2Hf_2O_7$:Pr ceramics before and after annealing (~1 mm thick; inset: their photos). Reproduced with permission from Ref. [42], © John Wiley and Sons 2014.

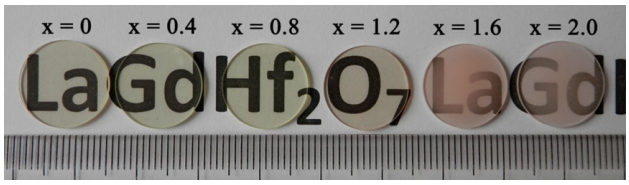

Fig. 12 Photograph of $La_{2-x}Gd_xHf_2O_7$ transparent ceramics vacuum sintered at 1830 ℃ for 6 h and annealed at 1500 ℃ for 5 h in air (1 mm thick). Reproduced with permission from Ref. [44], © Elsevier B.V. 2015.

(x =1.2). The thermally etched surface and fracture surface of the ceramics were shown in Fig. 13 and Fig. 14. Typically, the grain size sintered in vacuum was in micron scale and the main fracture mode was transgranular. As Gd content increased, the density of the ceramics linearly increased from 7.91 g/cm^3 (x = 0) to 8.88 g/cm^3 (x = 2.0). Meanwhile, the corresponding lattice parameters decreased linearly. With high density and high effective atomic number, the $La_{2-x}Gd_xHf_2O_7$ (x = 0–2.0) transparent ceramics are promising candidates for scintillator hosts.

5. 2 $A_2Zr_2O_7$ system transparent ceramics

In 2008, Murata Manufacturing Co., Ltd. reported in a US patent [60] that a series of $A_xB_yO_w$ translucent ceramics were fabricated by sintering in 98 vol% oxygen atmosphere. In their experimental examples, $La_2Zr_2O_7$, $Y_2Zr_2O_7$, $Gd_2Zr_2O_7$, and $La_{1.6}Y_{0.4}Zr_2O_7$, $La_{1.2}Y_{0.8}Zr_2O_7$, $La_{1.6}Gd_{0.4}Zr_2O_7$, $La_{1.2}Gd_{0.8}Zr_2O_7$, $La_{1.6}Yb_{0.4}Zr_2O_7$, $La_{1.6}Lu_{0.4}Zr_2O_7$, $La_2Zr_{1.6}Sn_{0.4}O_7$, etc. were presented. The sintered ceramics had low linear transmittance at 633 nm with a thickness of 0.4 mm. As they have higher refractive indices than conventional glass and plastics, they might be used in optical devices. In 2008, The Schott Company also applied a US patent [99], in which $A_{2+x}B_yD_zE_7$ series transparent ceramics were reported, like $Gd_2Zr_2O_7$ and $Gd_2(Hf, Zr)_2O_7$. The samples were firstly vacuum sintered at 1300 ℃ for 10 h with 10^{-5}–10^{-6} mbar vacuum degree, then HIPed at 1500 ℃ for 10 h with a pressure of 200 MPa. In the patent, other zirconates like $La_2Zr_2O_7$, $Y_2Zr_2O_7$, and $Yb_2Zr_2O_7$, etc., were also mentioned, but no detailed fabrication information was given.

In 2011, An *et al.* [45] fabricated $La_2Zr_2O_7$ transparent ceramic by reactive spark plasma sintering. The sintered body exhibited a pyrochlore structure and a uniform microstructure with the average grain size of 1.5 μm. The transmittance (Fig. 15) increased with increasing wavelength and reached 68% at 4–6 μm,

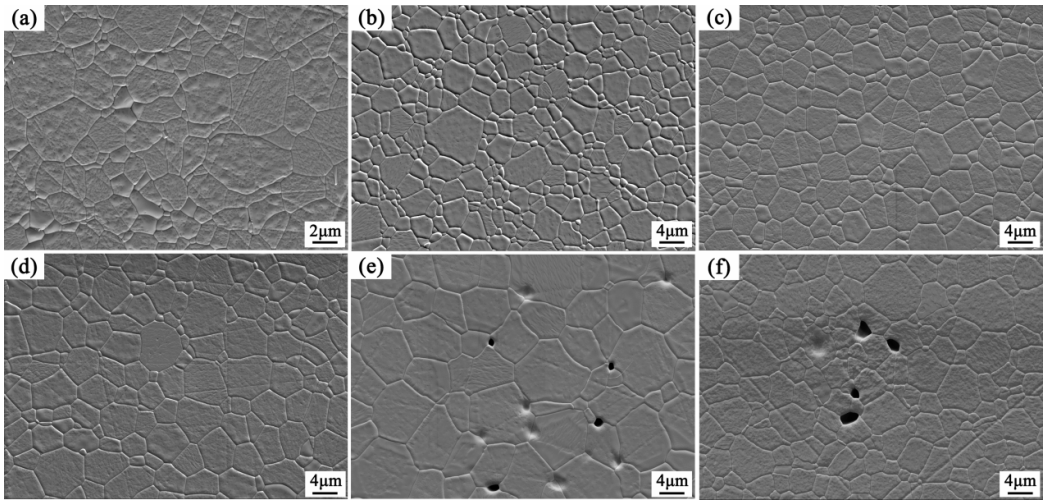

Fig. 13 Thermally etched surfaces of $La_{2-x}Gd_xHf_2O_7$ transparent ceramics: (a) x = 0; (b) x = 0.4; (c) x = 0.8; (d) x = 1.2; (e) x = 1.6; and (f) x = 2.0. Reproduced with permission from Ref. [44], © Elsevier B.V. 2015.

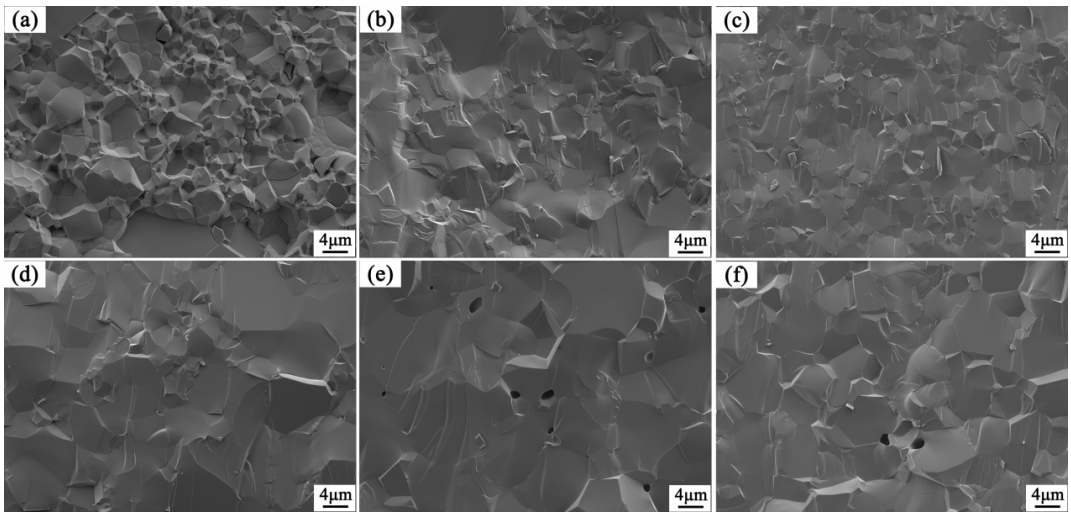

Fig. 14 Fracture surfaces of $La_{2-x}Gd_xHf_2O_7$ transparent ceramics: (a) x = 0; (b) x = 0.4; (c) x = 0.8; (d) x = 1.2; (e) x = 1.6; and (f) x = 2.0. Reproduced with permission from Ref. [44], © Elsevier B.V. 2015.

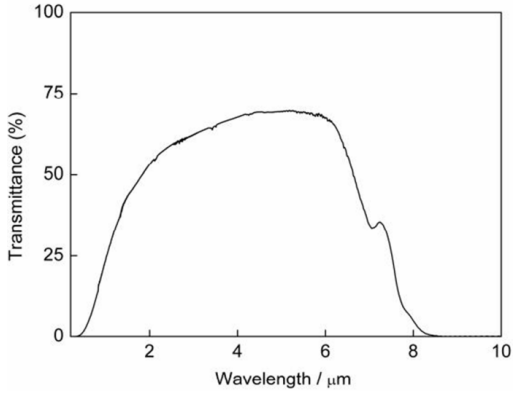

Fig. 15 Transmittance of $La_2Zr_2O_7$ transparent ceramic sintered at 1400 ℃ for 45 min (1 mm thick). Reproduced with permission from Ref. [44], © Trans Tech Publications, Switzerland 2011.

while the absorption edge in the infrared range was 8.5 μm. However, the transmittance in the visible range was relatively low. Zou *et al.* [83] fabricated $Y_2Zr_2O_7$ transparent ceramic by vacuum sintering at 1850 ℃ for 6 h from combustion-synthesized powders. The as-burnt $Y_2Zr_2O_7$ powders calcined at 1200 ℃ exhibited a defect fluorite structure and a porous morphology. The powders after being ball milled for 20 h can be sintered into transparent ceramics. The resultant ceramics show a pore-free microstructure and an in-line transmittance of 68% in the visible spectral region. On the other hand, Feng *et al.* [46] fabricated transparent $Nd_2Zr_2O_7$ ceramics by sintering in H_2 atmosphere at 1800 ℃ for 6–12 h using $Nd_2Zr_2O_7$ nanoparticles synthesized by combustion method. Emission at 1054.5 nm has been demonstrated using a laser diode pump at 800 nm, and the decay time is 460 μs, making $Nd_2Zr_2O_7$ transparent ceramic an excellent candidate for efficient high-power microchip lasers.

In 2013, Wang *et al.* [47,48] reported $La_{2-x}Gd_xZr_2O_7$ transparent ceramics. $La_{2-x}Gd_xZr_2O_7$ nanometric powders were synthesized by combustion method with glycine as the fuel. Then vacuum sintering was carried out to obtain the final transparent ceramics. With the increase of Gd^{3+} content, all the ceramics kept cubic pyrochlore structure, but the X-ray diffraction peaks shifted to higher angle as the lattice parameters became smaller. All the ceramics are transparent with high in-line transmittance and high refractive index (2.08 @ 632.8 nm, x = 0.4–1.6), indicating that $La_{2-x}Gd_xZr_2O_7$ ceramics might be used as optical lens. Moreover, with the increase of Gd^{3+} content, the effective atomic number and density of the ceramics increased, making them promising host candidates for scintillators. Then Eu^{3+} was chosen as the activator to study the luminescence properties of $La_{2-x}Gd_xZr_2O_7$:Eu^{3+} transparent ceramics (Fig. 16) [53]. They found that the cubic pyrochlore structure was not changed with the doping of 3 at% Eu^{3+}, while the cut-off edge of the transmittance curves and the luminescence behavior of the ceramics were affected by the annealing process as well as the Gd content. The cut-off edge shifted to opposite direction for the annealed and unannealed ceramics (Fig. 17). In addition, the luminescence intensity became stronger for the ceramics annealed in air. The doping of Gd^{3+} into La^{3+} site can change the energy band structure and the luminescence behavior was also adjusted. For ceramics annealed in air, the strongest luminescence

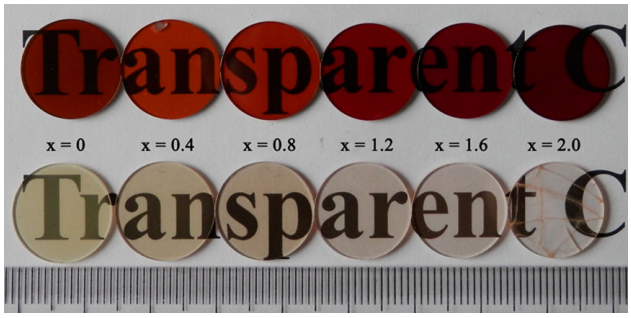

Fig. 16 Photograph of $La_{1.94-x}Gd_xZr_2O_7$:3at%Eu^{3+} (x = 0–2.0) transparent ceramics before (above) and after (below) annealing. Reproduced with permission from Ref. [53], © John Wiley and Sons 2015.

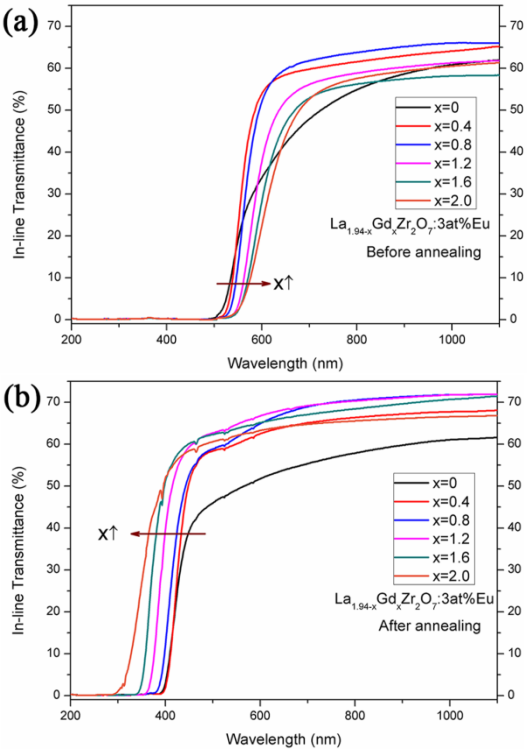

Fig. 17 Transmittance of $La_{1.94-x}Gd_xZr_2O_7$:3at%Eu^{3+} (x = 0–2.0) transparent ceramics (a) before and (b) after annealing. Reproduced with permission from Ref. [53], © John Wiley and Sons 2015.

peaks changed from 585 to around 630 nm due to the reduction of the crystal symmetry.

Further, $LaYZr_2O_7$ and $La_{2-x}Lu_xZr_2O_7$ transparent ceramics were prepared. Yi *et al.* [85] used slip casting to obtain the $LaYZr_2O_7$ green body and got $LaYZr_2O_7$ transparent ceramic by vacuum sintering at 1800 ℃ for 6 h. The obtained transparent ceramic has high transparency with a transmittance of 76.5% at 1100 nm, which was very close to the theoretical value (77.2%). Wang *et al.* [49] prepared $La_{2-x}Lu_xZr_2O_7$ transparent ceramics (Fig. 18) by solid state reactive sintering in vacuum. Surprisingly, with the increase of Lu content (x), phase transition from pyrochlore to defective fluorite occurred and a two-phase region existed in the range of x = 0.6–1.2 (Fig. 19). Grain sizes of the pyrochlore phase dominated samples (x < 0.5) were 11–14 μm, and that of the defective fluorite phase dominated samples were larger than 60 μm. However, grain sizes of the samples in the two-phase region were smaller than 3 μm (Fig. 20). The $La_{0.8}Lu_{1.2}Zr_2O_7$ ceramic with the smallest grain size (~2.5 μm) reached a highest in-line transmittance of 72.4% at 1100 nm among all the samples. According to Rayleigh–Gans–Debye scattering theory, when the refractive indices of the coexisting two phases are close to each other and the average grain size is smaller than 10 μm, the two phases have little influence on transparency of the ceramics.

5. 3 $A_2Ti_2O_7$ system transparent ceramics

Until now, research on $A_2Ti_2O_7$ transparent ceramics was not much, and the potential application is focused on optoceramics and imaging optics (optical elements).

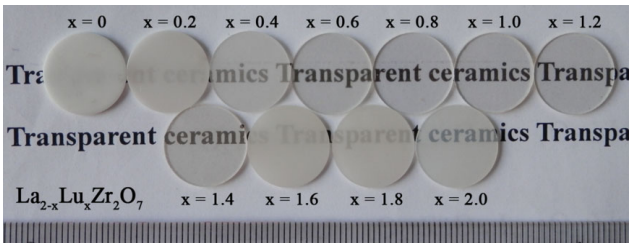

Fig. 18 Photograph of $La_{2-x}Lu_xZr_2O_7$ (x = 0–2.0) ceramics sintered at 1830 ℃ for 6 h in vacuum and annealed at 1500 ℃ for 5 h (1 mm thick). Reproduced with permission from Ref. [49], © Elsevier Ltd. 2014.

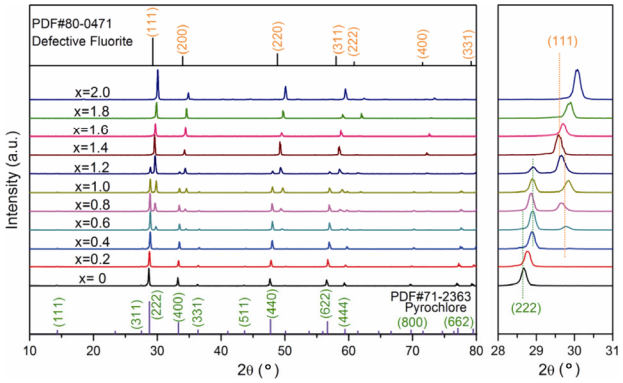

Fig. 19 XRD patterns of $La_{2-x}Lu_xZr_2O_7$ (x = 0–2.0) ceramics. Reproduced with permission from Ref. [49], © Elsevier Ltd. 2014.

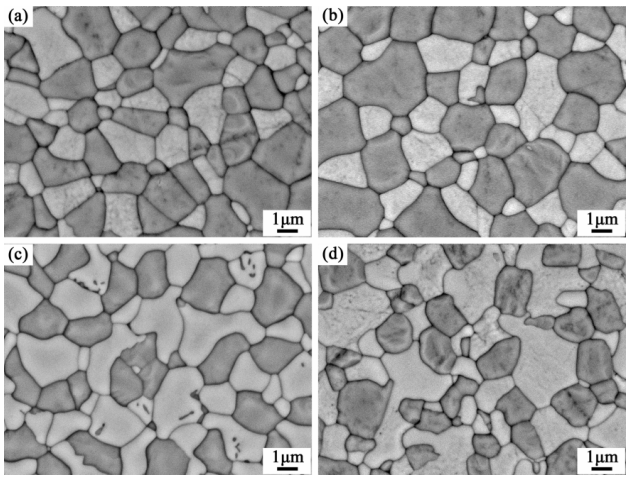

Fig. 20 Backscattered electron images of thermal-etched surfaces of $La_{2-x}Lu_xZr_2O_7$ ceramics: (a) x = 0.6, (b) x = 0.8, (c) x = 1.0, and (d) x = 1.2. Reproduced with permission from Ref. [49], © Elsevier Ltd. 2014.

As the melting temperature of $A_2Ti_2O_7$ compounds was lower than that of $A_2Hf_2O_7$ and $A_2Zr_2O_7$, the fabrication of $A_2Ti_2O_7$ transparent ceramics is expected to be easier with lower sintering temperature.

In 2008, The Schott Company applied a US patent [96] and reported $Y_2Ti_2O_7$, $Yb_2Ti_2O_7$, $Lu_2Ti_2O_7$, and $Gd_2Ti_2O_7$ transparent ceramics. However, the optical properties of these transparent ceramics were not given. Then in 2011, An *et al.* [50] prepared $Lu_2Ti_2O_7$ transparent ceramic by spark plasma sintering. The sintered body exhibited 72% transmittance at a wavelength of 2000 nm and 40% transmittance at 550 nm (Fig. 21). The average grain size was 14.5 μm with uniform microstructure. With cubic pyrochlore structure and high refractive index (2.57 at 632.8 nm), $Lu_2Ti_2O_7$ transparent ceramic is particularly suitable for application in an optical imaging system. Further work on improving the optical quality is needed. Moreover, other $A_2Ti_2O_7$ system transparent ceramics would be developed to enrich the application fields. Recently, Wang *et al.* [102] found that the addition of excess Y can improve the transparency of $Y_2Ti_2O_7$ transparent ceramics fabricated by solid state reactive sintering in vacuum. When the excess amount of Y to Ti is 2%, the highest in-line transmittance reached to 49.9% at 1100 nm (Fig. 22). In their newly unpublished work, the transparency of $Y_2Ti_2O_7$ transparent ceramic was greatly improved to 72.9% (0.5 mm thick) at 1100 nm by using powders synthesized by co-precipitation method.

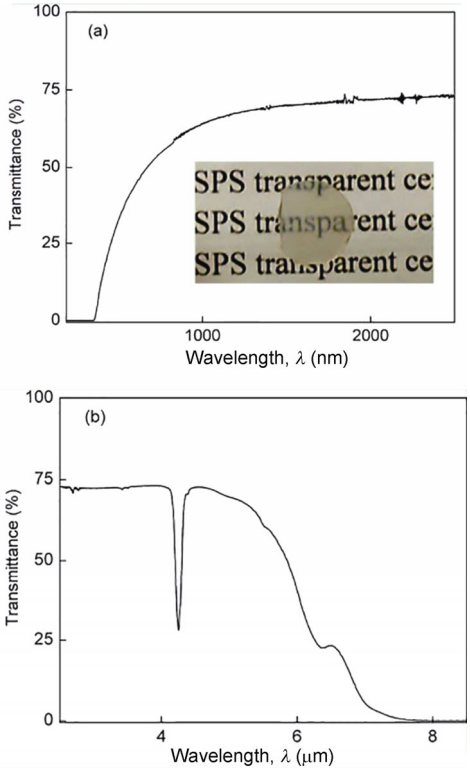

Fig. 21 Transmittance and photograph of $Lu_2Ti_2O_7$ transparent ceramic (0.8 mm thick). Reproduced with permission from Ref. [50], © Elsevier Ltd. 2010.

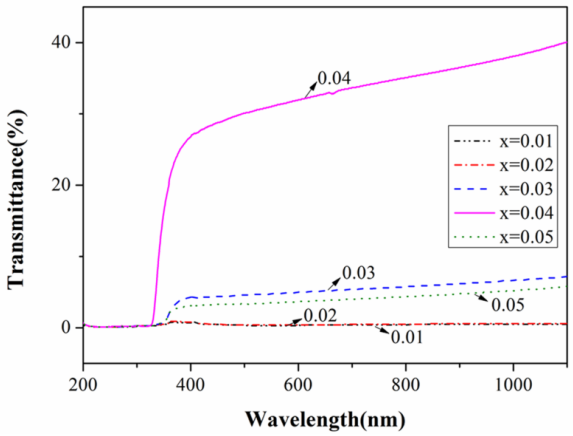

Fig. 22 Transmittance of $Y_{2+x}Ti_2O_{7+3x/2}$ ceramics vacuum sintered at 1600 ℃ for 6 h and annealed at 1000 ℃ for 6 h (0.5 mm thick). Reproduced with permission from Ref. [102], © Elsevier Ltd. 2018.

6 Potential applications

As a new series of transparent ceramics, $A_2B_2O_7$ system transparent ceramics are promising in fields such as lasers, camera lens, bulletproof windows or missile radome, and scintillators. However, there are

no practical applications up to now because the studies of $A_2B_2O_7$ system transparent ceramics are still in experimental stage.

The most potential application is scintillator, as most of the $A_2B_2O_7$ transparent ceramics have high density and high effective atomic number, which would gain high X-ray or γ-ray stopping power. The density increased in the order of $A_2Ti_2O_7$, $A_2Zr_2O_7$, and $A_2Hf_2O_7$, and thus the $A_2Hf_2O_7$ system transparent ceramics doping with proper rare earth ions are promising as a new series of transparent ceramic scintillators. However, the luminescence properties reported up to now were not attractive. On one hand, the luminescence intensity was not as high as the usual transparent ceramic scintillators. On the other hand, fast decay of Ce^{3+} and Pr^{3+} luminescence was not detected as expected in these ceramics. Chaudhry *et al.* [57] also came up with the idea that the Ce 5d state lies above the CBM (conduction band minimum), which would prevent any luminescence from the Ce site. In the study of $La_2Hf_2O_7$:Pr nanoceramics [42], no 5d→4f photoluminescence emission was observed, which was also explained that the lowest 5d level of Pr^{3+} was positioned within the conduction band of the host lattice. Only Pr^{3+} 4f→4f emission was observed means this type of transparent ceramic is promising to be used in X-ray excited scintillators.

Wang [56] studied the transmittance of $La_{2-x}Gd_xZr_2O_7$ and $La_{2-x}Gd_xHf_2O_7$ transparent ceramics in IR region, finding that the cut-off edges of the transmittance curve of these transparent ceramics were all larger than 8 μm. Compared with the IR cut-off edge of traditional transparent ceramics (AlON: ~5.55 μm; YAG: ~6.2 μm; Y_2O_3: ~9.4 μm; $MgAl_2O_4$: ~6.5 μm), these two system transparent ceramics have relatively wider IR transmission range, thus they may be new candidates for IR windows. The tested flexural strength and Vickers hardness of $LaGdZr_2O_7$ transparent ceramics were about 194 MPa and 10 GPa, which are higher than those of Y_2O_3 transparent ceramic. Except for excellent infrared optical properties, mechanical and thermal properties are also essential for IR window use, so further studies are needed.

In recent years, the increasing requirements from both sophisticated industrial as well as consumer mass markets have asked for optical transparent materials with extraordinary property combinations. For example, the continuous trend to miniaturization of digital photographic devices like digital cameras requires optical materials with very high refractive indices up to 2.0 or even higher, whereas industrial devices like optical microscopes require materials with special dispersion characteristics [6]. $A_2B_2O_7$ system transparent ceramics can be used as optical lens as they have high refractive index (higher than 2). The refractive index of $Y_2Hf_2O_7$, $La_{2-x}Gd_xZr_2O_7$, and $Lu_2Ti_2O_7$ was 2.018, 2.08, and 2.57, respectively. In 2012, Kintaka *et al.* [103] reported the optical properties of $La_2Zr_2O_7$ transparent ceramic and its abnormal partial dispersion when performed for optical use. The origin of the abnormal partial dispersion was investigated by measuring the vacuum ultraviolet reflectance and infrared absorption and by performing first-principle calculations. As the $A_2Ti_2O_7$ system have the highest refractive index among the $A_2B_2O_7$ system, more attentions would be paid on high refractive index optical elements applications of this kind of transparent ceramics.

In 2005, Gentleman and Clarke [104] found that Eu^{3+}doping into $Gd_2Zr_2O_7$ can give rise to strong luminescence as well as characteristic temperature-dependent luminescence lifetime at high temperatures. So they proposed the Eu^{3+}-doped materials could be employed in a number of different configurations for temperature sensing in thermal barrier coating systems. Recently, the luminescence properties of Pr^{3+}-doped $La_{0.4}Gd_{1.6}Zr_2O_7$ transparent ceramics were studied and continuous change in intensity ratio between the emission around 610 nm and the other bands (our unpublished data). Such an effect is appreciated in temperature sensing by changes in luminescence. Thus, $A_2B_2O_7$ system transparent ceramics with rare-earth ion doping could be new candidates as non-contact temperature sensors, and further study is in progress.

7 Conclusions and summary

Since the first fabrication of $La_2Hf_2O_7$ and $Gd_2Hf_2O_7$ transparent ceramics appeared in 2005, $A_2B_2O_7$ system transparent ceramics such as $A_2Hf_2O_7$, $A_2Zr_2O_7$, and $A_2Ti_2O_7$ have been developed for scintillator hosts as most of them have high density and effective atomic number, which would gain higher X-ray or γ-ray stopping power. In this review, the structure characteristic, powder synthesis method, ceramic sintering method, the reported $A_2Hf_2O_7$, $A_2Zr_2O_7$, and $A_2Ti_2O_7$ system transparent ceramics, and the potential applications of

$A_2B_2O_7$ system transparent ceramics were systematically summarized. In the near future, the applications on scintillators and optical elements would be focused continually, and newly developed applications such as temperature sensor, possible IR window, and optical lens would be further studied. The $A_2Hf_2O_7$ system transparent ceramics would be paid more attention on scintillator applications for their high density and high effective number. As the raw material prices of $A_2Zr_2O_7$ system transparent ceramics are relatively low, the researches on luminescence properties and the corresponding further application would be the key point. The $A_2Ti_2O_7$ system transparent ceramics tend to be used as optical elements for their higher refractive indices. Further studies are needed, including the fabrication of $A_2Ti_2O_7$ system transparent ceramics with optimized properties, including various refractive indices, Abbe numbers, and partial dispersions as well as high transmission and high property homogeneity.

Acknowledgements

The authors gratefully acknowledge the financial supports from the National Key R&D Program of China (No. 2017YFB0310500) and the National Natural Science Foundation of China (No. 51602326).

References

[1] Coble RL. Transparent alumina and method of preparation. U.S. Patent 3,026,210. 1962.

[2] Fang Y, Agrawal D, Skandan G, *et al*. Fabrication of translucent MgO ceramics using nanopowders. *Mater Lett* 2004, **58**: 551–554.

[3] Eilers H. Fabrication, optical transmittance, and hardness of IR-transparent ceramics made from nanophase yttria. *J Eur Ceram Soc* 2007, **27**: 4711–4717.

[4] Gupta TK, Rossing BR, Straub WD. Fabrication of transparent polycrystalline CaO. *J Am Ceram Soc* 1973, **56**: 339–339.

[5] Kortov VS, Milman II, Slesarev AI, *et al*. New BeO ceramics for TL ESR dosimetry. *Radiat Prot Dosim* 1993, **47**: 267–270.

[6] Peuchert U, Okano Y, Menke Y, *et al*. Transparent cubic-ZrO_2 ceramics for application as optical lenses. *J Eur Ceram Soc* 2009, **29**: 283–291.

[7] Tsukuma K. Transparent $MgAl_2O_4$ spinel ceramics produced by HIP post-sintering. *J Ceram Soc Jpn* 2006, **114**: 802–806.

[8] Dutta S, Gazza G. Hot pressing ceramic oxides to transparency by heating in isothermal increments. U.S. Patent 3,767,745. 1973.

[9] Zeman HD, Dibianca FA, Lovhoiden G. High-resolution X-ray imaging with a Gd_2O_3(Eu) transparent ceramic scintillator. In: *Proc. SPIE 2432, Medical Imaging 1995: Physics of Medical Imaging*, 1995: 454–461.

[10] Zou X, Yi H, Zhou G, *et al*. Highly transmitting ZrO_2-doped Lu_2O_3 ceramics from combustion synthesized powders. *J Am Ceram Soc* 2011, **94**: 2772–2774.

[11] Seeley ZM, Kuntz JD, Cherepy NJ, *et al*. Transparent Lu_2O_3:Eu ceramics by sinter and HIP optimization. *Opt Mater* 2011, **33**: 1721–1726.

[12] Qin X, Zhou G, Yang H, *et al*. Fabrication and plasma resistance properties of transparent YAG ceramics. *Ceram Int* 2012, **38**: 2529–2535.

[13] Qin X, Yang H, Zhou G, *et al*. Fabrication and properties of highly transparent Er:YAG ceramics. *Opt Mater* 2012, **34**: 973–976.

[14] Snow GS. Fabrication of transparent electrooptic PLZT ceramics by atmosphere sintering. *J Am Ceram Soc* 1973, **56**: 91–96.

[15] Duclos SJ, Greskovich CD, Lyons RJ, *et al*. Development of the HiLight^{TM} scintillator for computed tomography medical imaging. *Nucl Instrum Meth A* 2003, **505**: 68–71.

[16] Riedner RJ, Gürmen EO, Greskovich CD, *et al*. Solid state scintillator and treatment therefor. U.S. Patent 4,783,596. 1988.

[17] Yamada H, Suzuki A, Uchida Y, *et al.* A scintillator Gd_2O_2S:Pr, Ce, F for X-ray computed tomography. *J Electrochem Soc* 1989, **136**: 2713–2716.

[18] Van Eijk CWE. Inorganic scintillators in medical imaging. *Phys Med Biol* 2002, **47**: R85.

[19] Tsoukala VG, Greskovich CD. Hole-trap-compensated scintillator material. U.S. Patent 5,318,722. 1994.

[20] Lyberis A, Patriarche G, Gredin P, *et al*. Origin of light scattering in ytterbium doped calcium fluoride transparent ceramic for high power lasers. *J Eur Ceram Soc* 2011, **31**: 1619–1630.

[21] Lin W-Y, Hon M-H, Yang S-J. Effect of grain growth on hot-pressed optical magnesium fluoride ceramics. *J Am Ceram Soc* 1988, **71**: C-136–C-137.

[22] Basiev TT, Doroshenko ME, Fedorov PP, *et al*. Efficient laser based on CaF_2–SrF_2–YbF_3 nanoceramics. *Opt Lett* 2008, **33**: 521–523.

[23] Demidenko AA, Garibin EA, Gain SD, *et al*. Scintillation parameters of BaF_2 and BaF_2:Ce^{3+} ceramics. *Opt Mater* 2010, **32**: 1291–1293.

[24] Kuramoto N, Taniguchi H. Transparent AlN ceramics. *J Mater Sci Lett* 1984, **3**: 471–474.

[25] Chen F, Zhang F, Wang J, *et al*. Microstructure and optical properties of transparent aluminum oxynitride ceramics by hot isostatic pressing. *Scripta Mater* 2014, **81**: 20–23.

[26] Wang J, Zhang F, Chen F, *et al*. Fabrication of aluminum oxynitride (γ-AlON) transparent ceramics with modified gelcasting. *J Am Ceram Soc* 2014, **97**: 1353–1355.

[27] Mandal H. New developments in α-SiAlON ceramics. *J Eur Ceram Soc* 1999, **19**: 2349–2357.

[28] Chlique C, Merdrignac-Conanec O, Hakmeh N, *et al*. Transparent ZnS ceramics by sintering of high purity monodisperse nanopowders. *J Am Ceram Soc* 2013, **96**: 3070–3074.

[29] Colomban P, Havel M. Raman imaging of stress-induced phase transformation in transparent ZnSe ceramic and sapphire single crystals. *J Raman Spectrosc* 2002, **33**: 789–795.

[30] Kolesnikov NN, Kveder VV, Borisenko EB, *et al*. Structure and properties of CdTe ceramics produced through nanopowder compaction. *J Cryst Growth* 2005, **285**: 339–344.

[31] Fu-k'ang F, Kuznetsov AK, Keler ÉK. Zirconates of the rare earth elements and their physicochemical properties. Report 1. Zirconates of lanthanum, neodymium and cerium. *Russ Chem Bull* 1964, **13**: 1070–1075.

[32] Clarke DR, Phillpot SR. Thermal barrier coating materials. *Mater Today* 2005, **8**: 22–29.

[33] Zhang A, Lü M, Yang Z, *et al*. Systematic research on $RE_2Zr_2O_7$ (RE = La, Nd, Eu and Y) nanocrystals: Preparation, structure and photoluminescence characterization. *Solid State Sci* 2008, **10**: 74–81.

[34] Trojan-Piegza J, Zych E, Kosinska M. Fabrication and spectroscopic properties of nanocrystalline $La_2Hf_2O_7$:Pr. *Radiat Meas* 2010, **45**: 432–434.

[35] Eberman KW, Wuensch BJ, Jorgensen JD. Order–disorder transformations induced by composition and temperature change in $(Sc_zYb_{1-z})_2Ti_2O_7$ pyrochlores, prospective fuel cell materials. *Solid State Ionics* 2002, **148**: 521–526.

[36] Kim N, Grey CP. ^{17}O MAS NMR study of the oxygen local environments in the anionic conductors $Y_2(B_{1-x}B'_x)_2O_7$ (*B*, *B*' = Sn, Ti, Zr). *J Solid State Chem* 2003, **175**: 110–115.

[37] Uno M, Kosuga A, Okui M, *et al*. Photoelectrochemical study of lanthanide zirconium oxides, $Ln_2Zr_2O_7$ (Ln = La, Ce, Nd and Sm). *J Alloys Compd* 2006, **420**: 291–297.

[38] Yokoi H, Arita Y, Matsui T, *et al*. EXAFS study of $(La_{1-x}M_x)_2Zr_2O_7$ (M = Nd and Ce). *J Nucl Mater* 1996, **238**: 163–168.

[39] Ewing RC. Nuclear waste disposal–pyrochlore ($A_2B_2O_7$): Nuclear waste form for the immobilization of plutonium and "minor" actinides. *J Appl Phys* 2004, **95**: 5949–5971.

[40] Whittle KR, Cranswick LMD, Redfern SA, *et al.* Lanthanum pyrochlores and the effect of yttrium addition in the systems $La_{2-x}Y_xZr_2O_7$ and $La_{2-x}Y_xHf_2O_7$. *J Solid State Chem* 2009, **182**: 442–450.

[41] Ji Y, Jiang D, Fen T, *et al*. Fabrication of transparent $La_2Hf_2O_7$ ceramics from combustion synthesized powders. *Mater Res Bull* 2005, **40**: 553–559.

[42] Trojan-Piegza J, Gierlotka S, Zych E, *et al*. Spectroscopic studies of nanopowder and nanoceramics $La_2Hf_2O_7$:Pr scintillator. *J Am Ceram Soc* 2014, **97**: 1595–1601.

[43] Yi H, Zou X, Yang Y, *et al*. Fabrication of highly transmitting $LaGdHf_2O_7$ ceramics. *J Am Ceram Soc* 2011, **94**: 4120–4122.

[44] Wang Z, Zhou GH, Zhang F, *et al*. Fabrication and properties of $La_{2-x}Gd_xHf_2O_7$ transparent ceramics. *J Lumin* 2016, **169**: 612–615.

[45] An L, Ito A, Goto T. Fabrication of transparent $La_2Zr_2O_7$ by reactive spark plasma sintering. *Key Eng Mater* 2011, **484**: 135–138.

[46] Feng T, Clarke DR, Jiang D, *et al*. Neodymium zirconate ($Nd_2Zr_2O_7$) transparent ceramics as a solid state laser material. *Appl Phys Lett* 2011, **98**: 151105.

[47] Wang Z, Zhou G, Qin X, *et al*. Fabrication of $LaGdZr_2O_7$ transparent ceramic. *J Eur Ceram Soc* 2013, **33**: 643–646.

[48] Wang Z, Zhou G, Qin X, *et al*. Transparent $La_{2-x}Gd_xZr_2O_7$ ceramics obtained by combustion method and vacuum sintering. *J Alloys Compd* 2014, **585**: 497–502.

[49] Wang Z, Zhou G, Qin XP, *et al*. Fabrication and phase transition of $La_{2-x}Lu_xZr_2O_7$ transparent ceramics. *J Eur Ceram Soc* 2014, **34**: 3951–3958.

[50] An L, Ito A, Goto T. Highly transparent lutetium titanium oxide produced by spark plasma sintering. *J Eur Ceram Soc* 2011, **31**: 237–240.

[51] Ji Y, Jiang D, Shi J. Preparation and spectroscopic properties of $La_2Hf_2O_7$:Tb. *Mater Lett* 2005, **59**: 868–871.

[52] Ji Y, Jiang D, Shi J. $La_2Hf_2O_7$:Ti^{4+} ceramic scintillator for X-ray imaging. *J Mater Res* 2005, **20**: 567–570.

[53] Wang Z, Zhou G, Zhang J, *et al*. Effect of Gd content on luminescence properties of Eu^{3+}-doped $La_{2-x}Gd_xZr_2O_7$ transparent ceramics. *J Am Ceram Soc* 2015, **98**: 2476–2479.

[54] Wang Z, Zhou G, Zhang J, *et al*. Luminescence properties of Eu^{3+}-doped lanthanum gadolinium hafnates transparent ceramics. *Opt Mater* 2017, **71**: 5–8.

[55] Subramanian MA, Aravamudan G, Subba Rao GV. Oxide pyrochlores—A review. *Prog Solid State Chem* 1983, **15**: 55–143.

[56] Wang ZJ. Fabrication and properties of $Ln_2M_2O_7$ (M = Zr, Hf) transparent ceramics. Ph.D. Thesis. Beijing, China: University of Chinese Academy of Sciences, 2015.

[57] Chaudhry A, Canning A, Boutchko R, *et al*. First-principles studies of Ce-doped $RE_2M_2O_7$ (RE = Y, La; M = Ti, Zr, Hf): A class of non-scintillators. *J Appl Phys* 2011, **109**: 083708.

[58] Shimamura K, Arima T, Idemitsu K, *et al*. Thermophysical properties of rare-earth-stabilized zirconia and zirconate pyrochlores as surrogates for actinide-doped zirconia. *Int J Thermophys* 2007, **28**: 1074–1084.

[59] Blanchard PER, Clements R, Kennedy BJ, *et al*. Does local disorder occur in the pyrochlore zirconates? *Inorg Chem* 2012, **51**: 13237−13244.

[60] Hayashi T. Translucent ceramic, method for producing the same, optical component, and optical device. U.S. Patent 0,233,406. 2008.

[61] Mandal BP, Garg N, Sharma SM, *et al*. Preparation, XRD and Raman spectroscopic studies on new compounds $RE_2Hf_2O_7$ (*RE* = Dy, Ho, Er, Tm, Lu, Y): Pyrochlores or defect-fluorite? *J Solid State Chem* 2006, **179**: 1990–1994.

[62] Moreno KJ, Rodrigo RS, Fuentes AF. Direct synthesis of $A_2(Ti_{(1-y)}Zr_y)_2O_7$ ($A = Gd^{3+},Y^{3+}$) solid solutions by ball milling constituent oxides. *J Alloys Compd* 2005, **390**: 230–235.

[63] Moreno KJ, Fuentes AF, Garcıa-Barriocanal J, *et al*. Mechanochemical synthesis and ionic conductivity in the $Gd_2(Sn_{1-y}Zr_y)_2O_7$ ($0 \le y \le 1$) solid solution. *J Solid State Chem* 2006, **179**: 323–330.

[64] Jin D, Yu X, Yang H, *et al*. Hydrothermal synthesis and luminescence properties of Yb^{3+} doped rare earth stannates. *J Alloys Compd* 2009, **474**: 557–560.

[65] Gao L, An Y, Zhu H, *et al*. Hydrothermal synthesis and photoluminescence properties of $Y_2Zr_2O_7$:Tb^{3+} phosphors. *J Mater Sci* 2011, **46**: 1337–1340.

[66] Pavitra E, Seeta Rama Raju G, Yu JS. Solvothermal synthesis and luminescent properties of $Y_2Ti_2O_7$:Eu^{3+} spheres. *Phys Status Solidi RRL* 2013, **7**: 224–227.

[67] Mao Y, Park T-J, Zhang F, *et al*. Environmentally friendly methodologies of nanostructure synthesis. *Small* 2007, **3**: 1122–1139.

[68] Mao Y, Guo X, Huang JY, *et al*. Luminescent nanocrystals with $A_2B_2O_7$ composition synthesized by a kinetically modified molten salt method. *J Phys Chem C* 2009, **113**: 1204–1208.

[69] Shlyakhtina AV, Shcherbakova LG, Knotko AV. Studies of new order–disorder structural transitions in $Ln_2M_2O_7$ (Ln = Lu, Gd; M = Ti). *Ferroelectrics* 2003, **294**: 175–190.

[70] Shlyakhtina AV, Shcherbakova LG, Knotko AV, *et al*. Study of the fluorite–pyrochlore–fluorite phase transitions in $Ln_2Ti_2O_7$ (Ln = Lu, Yb, Tm). *J Solid State Electrochem* 2004, **8**: 661–667.

[71] Wan CL, Pan W, Xu Q, *et al*. Effect of point defects on the thermal transport properties of $(La_xGd_{1-x})_2Zr_2O_7$: Experiment and theoretical model. *Phys Rev B* 2006, **74**: 144109.

[72] Liu Z-G, Ouyang J-H, Zhou Y. Preparation and thermophysical properties of $(Nd_xGd_{1-x})_2Zr_2O_7$ ceramics. *J Mater Sci* 2008, **43**: 3596–3603.

[73] Zhou B-Z, Zhou G-H, An L-Q, *et al*. Morphology-controlled synthesis of yttrium hafnate by oxalate co-precipitation method and the growth mechanism. *J Alloys Compd* 2009, **481**: 434–437.

[74] LaCourse BC, Hardy AB, Rétot HL, *et al*. Ceramic scintillator body and scintillation device. U.S. Patent 0012787. 2012.

[75] Kido H, Komarneni S, Roy R. Preparation of $La_2Zr_2O_7$ by sol–gel route. *J Am Ceram Soc* 1991, **74**: 422–424.

[76] Li X, Cai H, Ding L, *et al*. Synthesis and luminescence properties of $La_2Ti_2O_7$:Er^{3+} nanocrystals with pyrochlore structure. *J Alloys Compd* 2012, **541**: 36–40.

[77] Saif M, Shebl M, Mbarek A, *et al*. Synthesis of non-toxic phosphor material based on pyrochlore-type dititanate (Eu^{3+}/$Y_2Ti_2O_7$). *J Photochem Photobiol A* 2015, **301**: 1–5.

[78] Tong Y, Xue P, Jian F, *et al*. Preparation and characterization of $Y_2Zr_2O_7$ nanocrystals and their photocatalytic properties. *Mat Sci Eng B* 2008, **150**: 194–198.

[79] Dhas NA, Patil KC. Combustion synthesis and properties of fine-particle rare-earth-metal zirconates, $Ln_2Zr_2O_7$. *J Mater Chem* 1993, **3**: 1289–1294.

[80] Liao Y, Jiang D, Ji YM, *et al*. Combustion synthesis of nanosized $Y_2Hf_2O_7$ and $Lu_2Hf_2O_7$ powders. *Key Eng Mater* 2005, **280–283**: 643–646.

[81] Zhang A, Lü M, Zhou G, *et al*. Combustion synthesis and photoluminescence of Eu^{3+},Dy^{3+}-doped $La_2Zr_2O_7$ nanocrystals. *J Phys Chem Solids* 2006, **67**: 2430–2434.

[82] Orlovskaya N, Chen Y, Miller N, *et al*. Glycine–nitrate synthesis of Sr doped $La_2Zr_2O_7$ pyrochlore powder. *Adv Appl Ceram* 2011, **110**: 54–57.

[83] Zou X, Zhou G, Yi H, *et al*. Fabrication of transparent $Y_2Zr_2O_7$ ceramics from combustion-synthesized powders. *J Am Ceram Soc* 2011, **94**: 1002–1004.

[84] Wang Z, Zhou G, Qin X, *et al*. Two-phase $LaLuZr_2O_7$ transparent ceramic with high transparency. *J Am Ceram Soc* 2014, **97**: 2035–2037.

[85] Yi H, Wang Z, Zhou G, *et al*. Highly transparent $LaYZr_2O_7$ ceramic fabricated by slip casting. *Ceram Int* 2016, **42**: 2070–2073.

[86] Zou X-Q, Zhou G-H, Yi H-L, *et al*. Fabrication of transparent $Y_2Hf_2O_7$ ceramic from combustion synthesized powders. *J Inorg Mater* 2011, **26**: 929–932.

[87] Zhou G, Wang Z, Zhou B, *et al*. Fabrication of transparent $Y_2Hf_2O_7$ ceramics via vacuum sintering. *Opt Mater* 2013, **35**: 774–777.

[88] Wang SF, Zhang J, Luo DW, *et al*. Transparent ceramics: Processing, materials and applications. *Prog Solid State Chem* 2013, **41**: 20–54.

[89] Ji YM. Exploration and luminescence properties of hafnate ceramic scintillators. Ph.D. Thesis. Shanghai Institute of Ceramics, Chinese Academy of Sciences, 2006.

[90] Zou XQ. Fabrication and luminescence properties of $RE_2Hf_2O_7$/$RE_2Zr_2O_7$ transparent ceramics. Master Thesis. Shanghai Institute of Ceramics, Chinese Academy of Sciences, 2011.

[91] Anselmi-Tamburini U, Woolman JN, Munir ZA. Transparent nanometric cubic and tetragonal zirconia obtained by high-pressure pulsed electric current sintering. *Adv Funct Mater* 2007, **17**: 3267–3273.

[92] Galusek D, Sedláček J, Chovanec J, *et al*. The influence of MgO, Y_2O_3 and ZrO_2 additions on densification and grain growth of submicrometre alumina sintered by SPS and HIP. *Ceram Int* 2015, **41**: 9692–9700.

[93] Reimanis I, Kleebe H-J. A review on the sintering and microstructure development of transparent spinel ($MgAl_2O_4$). *J Am Ceram Soc* 2009, **92**: 1472–1480.

[94] Gan L, Park Y-J, Kim H, *et al*. Fabrication of submicron-grained IR-transparent Y_2O_3 ceramics from commercial nano-raw powders. *Ceram Int* 2015, **41**: 11992–11998.

[95] Serivalsatit K, Ballato J. Submicrometer grain-sized transparent erbium-doped scandia ceramics. *J Am Ceram*

Soc 2010, **93**: 3657–3662.
[96] Peuchert U, Menke Y. Optoceramics, optical elements manufactured thereof and their use as well as imaging optics. U.S. Patent 7,710,656. 2010.
[97] Lu TC, Chang XH, Qi JQ, *et al*. Low-temperature high-pressure preparation of transparent nanocrystalline $MgAl_2O_4$ ceramics. *Appl Phys Lett* 2006, **88**: 213120.
[98] Hreniak D, Bettinelli M, Speghini A, *et al*. The f–f emission of Pr^{3+} ion as an optical probe for the structural properties of YAG nanoceramics. *J Nanosci Nanotechnol* 2009, **9**: 6315–6319.
[99] Peuchert U, Menke Y. Active optoceramics with cubic crystal structure, method of production of the optoceramics, and uses thereof. U.S. Patent 8,197,711. 2012.
[100] Borisevich A, Korzhik M, Lecoq P. Luminescence of Ce doped oxygen crystalline compounds based on Hf and Ba. *Nucl Instrum Meth A* 2003, **497**: 206–209.
[101] Birxner LH. Structural and luminescent properties of the $Ln_2Hf_2O_7$-type rare earth hafnates. *Mat Res Bull* 1984, **19**: 143–149.
[102] Wang X, Xie J, Wang Z, *et al*. Fabrication and properties of $Y_2Ti_2O_7$ transparent ceramics with excess Y content. *Ceram Int* 2018, **44**: 9514–9518.
[103] Kintaka Y, Hayashi T, Honda A, *et al*. Abnormal partial dispersion in pyrochlore lanthanum zirconate transparent ceramics. *J Am Ceram Soc* 2012, **95**: 2899–2905.
[104] Gentleman MM, Clarke DR. Luminescence sensing of temperature in pyrochlore zirconate materials for thermal barrier coatings. *Surf Coat Technol* 2005, **200**: 1264–1269.